SciEn
Journal of Engineering Advancements Vol. 03(01) 2022, pp 012-022 https://doi.org/10.38032/jea.2022.01.003

Evaluation of Different Turbulence Models at Low Reynolds Number for the Flow over Symmetric and Cambered Airfoils

Tafsirul Hassan, Md. Tazul Islam, Md. Mizanur Rahman, Abu Raihan Ibna Ali, Asif Al Ziyan*

Department of Mechanical Engineering, Chittagong University of Engineering & Technology, Chattogram-4349, Bangladesh

Received: February 13, 2022, Revised: March 16, 2022, Accepted: March 16, 2022, Available Online: March 18, 2022

ABSTRACT

This paper presents an evaluation of five different turbulence models by comparing the numerical data derived from these models using ANSYS Fluent with experimental data at a Reynolds number and a Mach number of 0.05×10^6 and 0.015 respectively based on the centerline chord of the airfoil for the flow over NACA 0012 and NACA 2412 airfoils. Moreover, the aim of the present study is to demonstrate the difference in aerodynamic characteristics of the airfoils in order to find aerodynamically more advantageous airfoil. It is concluded that Spalart-Allmaras model and k-ω SST model are capable of providing the most accurate prediction for lift coefficient at a low angle of attack for both airfoils. Standard k - ε model gives a slightly low value of lift coefficient at low angle of attack and slightly high value of lift coefficient at high angle of attack for both airfoils. k-ω SST model, Spalart-Allmaras model, Transition k-k_L - ω model, and γ-$R\tilde{e}_\theta$ Transition SST model can predict drag coefficient reasonably at low angle of attack. At a high angle of attack, however, no turbulence model is able to give a satisfactory prediction for lift coefficient as well as drag coefficient, which implies that these models are unable to predict post-stall characteristics. NACA 2412 airfoil produces more lift coefficient than that of the NACA 0012 airfoil at all angles of attack. Moreover, the drag coefficient of NACA 2412 airfoil is less than that of the NACA 0012 airfoil, which implies that NACA 2412 airfoil exhibits better aerodynamic performance. The lift to drag coefficient ratio of NACA 2412 airfoil is also higher than that of the NACA 0012 airfoil indicating NACA 2412 airfoil to be more fuel economic.

Keywords: Turbulence Models, CFD Analysis, Wind Tunnel Testing, Airfoil, Lift Coefficient, Drag Coefficient.

1 Introduction

Aerodynamics is one of the important branches of science that deals with the analysis of airflow over a body. The investigation of airflow characteristics over airfoils is inevitable during designing aircraft wings, helicopter rotors, wind turbines, etc. Different approaches such as numerical, analytical, experimental, etc. approaches are followed in any investigation. These approaches have their own pros and cons. Nowadays, computational fluid dynamics (CFD) simulation is gaining enormous popularity, since wind tunnel testing is quite laborious and costly compared to CFD. Hence, the numerical method is the best alternative to the experimental method [1]. It would be more convenient if a turbulence model could predict the aerodynamic performance of an airfoil that would be close to experimental outcomes. CFD is a division of fluid mechanics that utilizes numerical analysis in order to solve and analyze a problem related to fluid flow [2],[3]. It necessitates a governing equation. In CFD analysis, a CAD model is first generated in CAD software, which is then imported into CFD software. Mesh is generated and a proper turbulence model is selected to predict quantitative and qualitative aerodynamic characteristics. Different boundary conditions and convergence criteria are set. Then simulation is initialized and run to obtain numerical results. The key premise of practically all CFD issues is the Navier-Stokes equations. The terms comprising viscous activities are eliminated in order to convert Navier-Stokes equations to Euler equations. In order to obtain linearized potential equations, these equations are then manipulated. Two-dimensional (2D) methods were developed in the 1930s [4]. There are three governing equations upon which all of the fluid dynamics are based: (a) Mass is conserved. (b) The rate of change of momentum is constant and (c) Energy is conserved. These governing equations can be solved by using either the finite element method or the finite volume method [5].

Sahoo and Maity [6] found k-ω SST turbulence model to be more accurate at a high Reynolds number of 6×10^6 compared to other turbulence models. Maani et al. [7] also concluded that there was good consistency between k-ω SST model and reliable experimental data for the compressible flow of high Reynolds number. Badran [8] showed that the RNG k-ε model and Reynolds Stress Model (RSM) had the ability to capture the physics of unsteady flow and these models showed excellent agreement with experimental data to predict pressure coefficient, skin friction, velocity vectors, shear stress, and kinetic energy. Oukassou et al. [9] found that Spalart-Allmaras, RNG k-ε model, and k-ω model were in good agreement with experimental outputs. Douvi et al. [10] concluded that k-ω SST model is more consistent than any other turbulence model at a moderate Reynolds number of 3×10^6 and at a low angle of attack while no turbulence model can provide satisfactory prediction at a high angle of attack. Linjing et al. [11] simulated for S825 and S827 2-D wind turbine with Spallart-Allmaras model, Standard k-ω model, and standard k-ε model and concluded that these models cannot provide accurate prediction for the stall characteristics at high angle of attack. Bacha and Ghaly [12] presented a transition model which reflected a significant improvement in drug prediction at low Reynolds numbers.

The NACA 2412 airfoil is a cambered airfoil and has a maximum camber of 0.02 times chord, which is positioned 0.4 times chord from the leading edge having a maximum thickness of 0.12 times chord. The NACA 0012 airfoil is a symmetric airfoil having a maximum thickness of 0.12 times chord with no

*Corresponding Author Email Address: tafsir2086@gmail.com Published by: SciEn Publishing Group

camber. NACA 0012 airfoils have been used as a reference for the evaluation of wall interference and correction technique. Moreover, they are used as helicopter rotors, rudders, and flaps in the airplane while NACA 2412 airfoils, slow-speed airfoils, are used in the single-engine Cessna 152, 172, and 182 airplanes [13],[14]. Mayer et al. [15] investigated the effect of flow separation of a NACA 0012 airfoil for a range of Reynolds numbers and angles of attack. They observed that the main contributing eddies causing unsteady surface pressure fluctuations move away from the airfoil surface once the flow has separated. Harish et al. [16] studied the prediction of stalling angle by analysis of flow over symmetric airfoil NACA 0012 using reference velocity 01 m/s and concluded that an increase in lift force by 32.32% was observed for 12° angle of attack as compared to 4° angle of attack. Patil and Thakare [17] showed the variation of performance of NACA 0012 airfoil with Reynolds number. NACA0012 provided maximum lift at a high Reynolds number. Hasegawa and Sakaue [18] showed that almost 50% drag was reduced because of using microfiber coating over NACA 0012 airfoil compared to a surface without being coated with microfiber at the Reynolds number of 6.1×10^4. Venkatesan et al. [19] conducted a computational analysis of aerodynamic characteristics of dimple airfoil NACA 2412 airfoil at various angles of attack. They explained that dimples enhance the lift of an airfoil and square dimples had yielded better results. Meghani [20] observed that there was appreciable separation observed to develop at 20% of the chord of NACA 2412 airfoil while conducting wind tunnel test which XFOIL and FLUENT weren't capable to show. It was also concluded that XFOIL was suitable for analysis only at a low Reynolds number (Re=500,000). At high Reynolds number, XFOIL results were not found to be accurate for full-scale flow. Havaldar et al. [21] concluded that the lift coefficient for NACA 2412 airfoil with internal passage was higher than the lift coefficient for NACA 2412 airfoil. They showed that the point of separation for NACA 2412 airfoil with internal passage was shifted towards the trailing edge that reducing the boundary layer separation at a higher angle of attack from the airfoil.

Many researchers have attempted to evaluate turbulence models at moderate and high Reynolds numbers. However, very few studies focused on evaluation at low Reynolds number, although aerodynamic characteristics at low Reynolds number are important for low-speed light aircraft, particularly, during takeoff and landing. This study addresses the research gap. The main aim of the present study is to determine a more suitable and accurate turbulence model that has the capability of predicting aerodynamic flow characteristics at low Reynolds number as well as Mach number for the flow over both symmetric and cambered airfoils. In this present study, five different turbulence models are used for numerical analysis of symmetric airfoil NACA 0012 and cambered airfoil NACA 2412 using ANSYS Fluent [22], a renowned CFD software. k-ω SST model (2 equations), Standard k-ε model (2 equations), Spalart-Allmaras model (1 equation), Transition k-k_L-ω model (3 equations) and $\gamma - Re_\theta$ Transition SST model (4 equations) are applied to predict the quantitative and qualitative performance of the airfoils with suitable boundary conditions at a Reynolds number and a Mach number of 0.05×10^6 and 0.015 respectively based on the centerline chord of the airfoil. In addition, wind tunnel testing is conducted at the Reynolds number and Mach number same with the numerical investigation to evaluate different turbulence models. The focus of the present study is on the dynamic parameters such as lift coefficient, drag coefficient, etc. Finally, a comparison of aerodynamic characteristics between NACA 0012 and NACA 2412 airfoil is also presented in order to demonstrate aerodynamically more advantageous airfoil.

2 Materials and Methods

2.1 Preparing the CAD models in DesignModeler

DesignModeler [22] has been used to prepare CAD models of the airfoil geometries and flow domain. The coordinates of the airfoils are imported to the software and the geometries with flow filed are modeled. Upstream and downstream are taken as 12.5 times chord length. Fig. 1 illustrates the geometry of the flow domain of the airfoils.

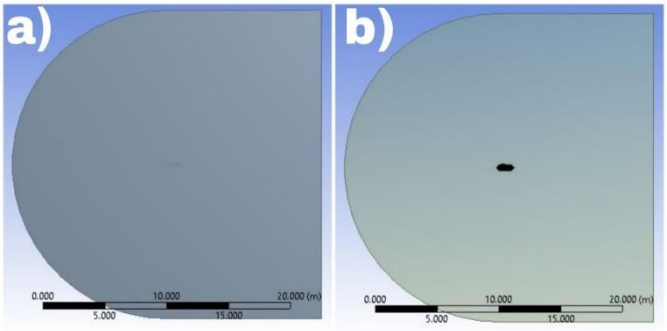

Fig. 1 CAD models of the flow domain of (a) NACA 0012 and (b) NACA 2412 airfoil.

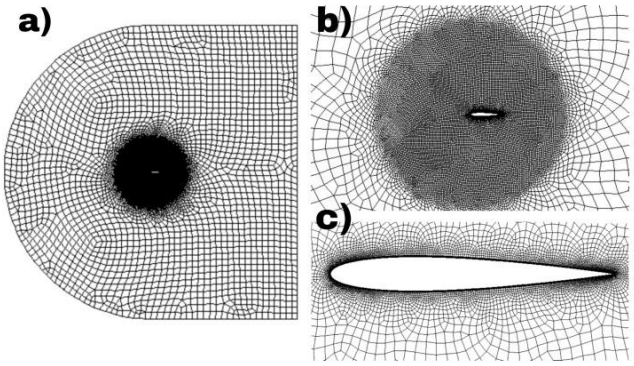

Fig. 2 Mesh of (a) whole flow domain, (b) flow domain near sphere of influence, (c) flow domain near NACA 0012 airfoil.

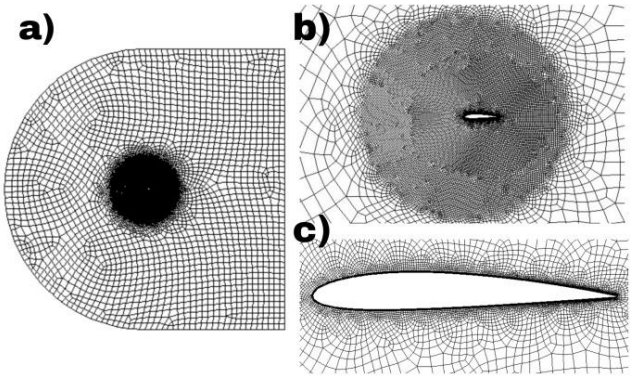

Fig. 3 Mesh of (a) whole flow domain, (b) flow domain near sphere of influence, (c) flow domain near NACA 2412 airfoil.

2.2 Mesh Generation

The 2-D CAD models of the flow geometries are imported to ANSYS Fluent. The mesh for both of the geometry of the airfoil is of unstructured type. The cells of the meshes are

quadrilateral and mesh matric has orthogonal quality. The element is 50% of the chord and the element order is linear. The edge sizing of the airfoil is a bias type of bidirectional having a bias factor of 10 and element size of 0.3% of chord. Smooth transition with 1.2 growth rate inflation is taken near the surfaces of the airfoils. The layers of inflation are 10 and the maximum thickness is 0.6% of the chord. For body sizing, a sphere of influence of radius of 300% of chord and element size of 5% of the chord is taken where the center of the radius of the sphere of influence is at the origin of the global coordinate system. The maximum Y^+ value used in this study is approximately 0.4. A Y^+ value of the size should be sufficient to perfectly resolve the inner part of the boundary layer. A domain with a high grid number leads to an accurate simulated result. However, usage of higher grid numbers results in high computational costs. Hence, the lift coefficient at an angle of attack of 0° for a various number of elements is determined. It is observed that lift coefficients are approximately the same for the element number higher than 25000. Considering computational cost as well as the accuracy of simulation, nodes, and elements of NACA 0012 airfoil have been taken as 27343 and 26962 respectively while nodes and elements of NACA 2412 airfoil have been taken as 26414 and 26040 respectively. Fig. 2 and Fig. 3 demonstrate the mesh of the flow domain of NACA 0012 airfoil and NACA 2412 airfoil respectively.

2.3 Governing Equations

Conservation of Mass:

Equation (1) represents the continuity equation. It is a common form of conservation of mass equation, which is valid for not only incompressible flow but also compressible flow.

$$\frac{\partial \rho}{\partial t} + \nabla \cdot (\rho \vec{u}) = s_m \tag{1}$$

where, the source s_m represents the mass that is added to the continuous phase from the dispersed second phase and any user-defined source.

Conservation of Momentum:

Equation (2) represents the conservation of momentum.

$$\frac{\partial}{\partial t}(\rho \vec{u}) + \nabla \cdot (\rho \vec{u}\vec{v}) = -\nabla p + \nabla \cdot \bar{\bar{\tau}} + \rho \vec{g} + \vec{F} \tag{2}$$

Where, p is the static pressure, $\rho \vec{g}$ is the gravitational body force, $\vec{F}$ is the external body force and $\bar{\bar{\tau}}$ is the stress tensor which is expressed as:

$$\bar{\bar{\tau}} = \mu \left[(\nabla \vec{u} + \nabla \vec{u}^T) - \frac{2}{3} \right] \nabla . \vec{u} I \tag{3}$$

where, I is the unit tensor, and μ is the molecular viscosity.

Equations in 2-D:

The continuity equation for the 2-Dimensional, incompressible and steady flow can be expressed as:

$$\frac{\partial u}{\partial x} + \frac{\partial v}{\partial y} = 0 \tag{4}$$

The momentum equations for viscid flow in two dimensions are respectively,

$$\rho \frac{Du}{Dt} = -\frac{\partial p}{\partial x} + \frac{\partial \tau_{xx}}{\partial x} + \frac{\partial \tau_{yx}}{\partial y} + \rho f_x \tag{5}$$

$$\rho \frac{Du}{Dt} = -\frac{\partial p}{\partial y} + \frac{\partial \tau_{xy}}{\partial x} + \frac{\partial \tau_{yy}}{\partial y} + \rho f_y \tag{6}$$

2.3.1 The k-ω SST Turbulence Model

Standard k-ω model was developed from Wilcox's [23] k-ω model which was modified by Menter [24] creating a new turbulence model named k-ω Shear-Stress Transport (SST) model possessing two equations. This new model is more perfect and consistent than the Standard k-ω model for a broader class of fluid flows.

The k-ω SST turbulence model is governed by the following equations.

$$\frac{D\rho k}{Dt} = \tau_{ij} \cdot \frac{\partial u_i}{\partial x_j} + \beta^* \rho \omega k + \frac{\partial}{\partial x_j}\left[\left(\mu_{+\sigma_k} \mu_t\right) \frac{\partial k}{\partial x_j} \right] \text{`and} \tag{7}$$

$$\frac{D\rho\omega}{Dt} = \frac{\gamma}{\nu_t}\tau_{ij}\frac{\partial u_i}{\partial x_j} - \beta\rho\omega^2 + \frac{\partial}{\partial x_j}\left[\left(\mu_{+\sigma_\omega} \mu_t\right) \frac{\partial \omega}{\partial x_j} \right] + 2\rho(1-F_1)\sigma_\omega \frac{1}{\omega}\frac{\partial k}{\partial x_j}\frac{\partial \omega}{\partial x_j} \tag{8}$$

where,

$\beta^* = \frac{\varepsilon}{k\omega}$ and the turbulence stress tensor is

$$\tau_{ij} = -\rho \overline{u_i' u_j'} = \mu_t \left(\frac{\partial u_i}{\partial x_j} + \frac{\partial u_j}{\partial x_i} - \frac{2}{3}\frac{\partial u_k}{\partial x_k}\delta_{ij} \right) - \frac{2}{3}\rho k \delta_{ij}. \tag{9}$$

The turbulence viscosity can be determined by $\nu_t = a_1 \frac{k}{\max[a_1 \omega, \Omega F_2)}$

where, Ω = the absolute value of the vorticity, a_1 =31 .01 and the function F_2 is given by

$$F_2 = tan\, h\left\{ \left[max\left(\frac{2\sqrt{k}}{0.09\omega y}, \frac{500\nu}{y^2\omega} \right) \right] \right\}^2 \tag{10}$$

where, y is the distance to the nearest surface.

The coefficients $\beta, \gamma, \sigma_k, \sigma_\omega$ are defined as functions of the coefficients of the k-ω model which are defined as follows:

$$\begin{aligned} &\beta = F_1\beta_1 + (1-F_1)\beta_2, \gamma = F_1\gamma_1 + (1-F_1)\gamma_2 \\ &\sigma_k = F_1\sigma_{k_1} + (1-F_1)\sigma_{k_2}, \sigma_\omega = F_1\sigma_{\omega_1} + (1-F_1)\sigma_{\omega_2} \end{aligned} \tag{11}$$

where the function F_1 is

$$F_1 = tanh\left\{ \left[min\left[max\left(\frac{\sqrt{k}}{0.09\omega y}, \frac{500\nu}{y^2\omega} \right), \frac{4\rho\sigma_{\omega_2} k}{CD_{k\omega} y^2} \right] \right]^4 \right\} \tag{12}$$

and the coefficient

$$CD_{k\omega} = max\left(2\rho\sigma_{\omega_2} \frac{1}{\omega}\frac{\partial k}{\partial x_j}\frac{\partial \omega}{\partial x_j}, 10^{-20} \right). \tag{13}$$

Model constants:

β^* =0.09, β_1=0.075, β_2 =0.0828, γ_1=0.5532, γ_2=0.4404, σ_{k_1}=0.85, σ_{k_2}=1.0, σ_{ω_1}=0.5 and σ_{ω_1}=0.856.

2.3.2 Standard k-ε Model

Launder and Spalding [25] proposed a turbulence model that involves two equations. The model is popularly known as the standard k-ε model and is the most widely-used engineering turbulence model which is robust and reasonably accurate. The standard k-ε model is valid only for fully developed turbulent flows. Some modifications have been made over time to this model. These modified models include the RNG k-ε model and the realizable k-ε model [26]. Enhanced wall function was used

as ε equation contains a term which cannot be calculated without wall function.

The transport equation for turbulent kinetic energy (k) is

$$\frac{\partial(\rho k)}{\partial t}+\frac{\partial(\rho k u_i)}{\partial x_i}=\frac{\partial}{\partial x_j}\left[\left(\mu+\frac{\mu_t}{\sigma_k}\right)\frac{\partial k}{\partial x_j}\right]+G_k+G_b-\rho\varepsilon-Y_M+S_k \quad (14)$$

and transport equation for turbulent dissipation rate (ε) is

$$\frac{\partial(\rho\varepsilon)}{\partial t}+\frac{\partial(\rho\varepsilon u_i)}{\partial x_i}=\frac{\partial}{\partial x_j}\left[\left(\mu+\frac{\mu_t}{\sigma_\varepsilon}\right)\frac{\partial \varepsilon}{\partial x_j}\right]+C_{1\varepsilon}\frac{\varepsilon}{k}(G_k+C_{3\varepsilon}G_b)-C_{2\varepsilon}\rho\frac{\varepsilon^2}{k}+S_\varepsilon \quad (15)$$

where, μ_t = turbulent viscosity $= \rho C_\mu \frac{k^2}{\varepsilon}$, G_k = generation of the turbulent kinetic energy due to the mean velocity gradient, σ_k = effective prandtl number for turbulent kinetic energy, σ_ε = effective prandtl number for rate of dissipation, $C_{1\varepsilon}, C_{2\varepsilon}$ are constants

Model Constants:

The default values of model constants $C_{1\varepsilon}, C_{2\varepsilon}, C_\mu, \sigma_k, and\ \sigma_\varepsilon$ determined from experiments for fundamental turbulent flows and have the following values.

$$C_{1\varepsilon}=1.44, C_{2\varepsilon}=1.92, C_\mu=0.09, \sigma_k=1.0, \sigma_\varepsilon=1.3$$

2.3.3 Spalart-Allmaras Model

Spalart-Allmaras model is a one equation turbulence model that was proposed by Spalart and Allmarus [27]. It was mainly designed for applications that involve aerodynamic operations while it is now also being used in turbomachinery applications. This model solves a transport equation that involves kinematic eddy viscosity. The main advantage of this model is that it is relatively robust. The resolution requirement is moderate. It is quite stable and it also shows good convergence.

The transported variable in the Spalart-Allmaras model, $\tilde{\nu}$, is identical to the turbulent kinematic viscosity except in the near-wall (viscosity-affected) region. The transport equation for $\tilde{\nu}$ is

$$\frac{\partial}{\partial t}(\rho\tilde{\nu})+\frac{\partial}{\partial x_i}(\rho\tilde{\nu}u_i)=G_\nu+\frac{1}{\sigma_{\tilde{\nu}}}\left[\frac{\partial}{\partial x_j}\cdot\left\{(\mu+\rho\tilde{\nu})\frac{\partial\tilde{\nu}}{\partial x_i}\right\}+C_{b2}\rho\left(\frac{\partial\tilde{\nu}}{\partial x_j}\right)^2\right]-Y_\nu+S_{\tilde{\nu}} \quad (16)$$

where, G_ν = the production of turbulent viscosity, Y_ν = the destruction of turbulent viscosity that occurs in the near-wall region due to wall blocking and viscous damping, ν = the molecular kinematic viscosity, $S_{\tilde{\nu}}$ = a user-defined source term and $\sigma_{\tilde{\nu}}$ and C_{b2} are the constants.

Model constants:

$$C_{b2}=0\cdot622, \sigma_{\tilde{\nu}}=\frac{2}{3}$$

2.3.4 Transition k-k$_L$-ω Model

Walter and Cokljat [28] developed a three equation k-k$_L$- ω turbulence model which was inspired by the idea that was introduced by Walters and Leylek [29]. The model can successfully predict boundary layer development and transition flow behavior in various fluid systems.

The k-k$_L$-ω model is considered to be a three-equation eddy-viscosity type, which includes transport equations for turbulent kinetic energy (k_T), laminar kinetic energy (k_L), and the inverse turbulent time scale (ω).

$$\frac{Dk_T}{Dt}=P_{k_T}+R+P_{N\,AT}-\omega k_T-D_T+\frac{\partial}{\partial x_j}\left[\left(\nu+\frac{\alpha_T}{\alpha_k}\right)\frac{\partial k_T}{\partial x_j}\right] \quad (17)$$

$$\frac{Dk_L}{Dt}=P_{k_L}-R-R_{N\,AT}-D_L+\frac{\partial}{\partial x_j}\left[\nu\frac{\partial k_L}{\partial x_j}\right] \quad (18)$$

$$\frac{D_\omega}{D_t}=C_{\omega1}\frac{\omega}{k_T}p_{k_T}+\left(\frac{C_{\omega R}}{f_W}-1\right)\frac{\omega}{k_T}(R+R_{N\,AT})-C_{\omega2}\omega^2+C_{\omega3}f_\omega\alpha_T f_W^2\frac{\sqrt{k_T}}{d^3}+\frac{\partial}{\partial x_j}\left[\left(\nu+\frac{\alpha_T}{\alpha_\omega}\right)\frac{\partial\omega}{\partial x_j}\right] \quad (19)$$

Model constants:

$$C_{\omega1}=0.44, C_{\omega2}=0.92, C_{\omega3}=0.3$$

2.3.5 $\gamma - Re_\theta$ Transition SST Model

$\gamma - Re_\theta$ transition SST model was developed subsequently by Menter and Langratry [30]-[32]. It had successfully been used for flow prediction of an expansion swirl flow [33]. The transition SST model is based on the coupling of the SST k-ω transport equations with two other transport equations, one for the intermittency and one for the transition onset criteria, in terms of momentum-thickness Reynolds number.

The transport equation for the intermittency γ is defined as

$$\frac{\partial(\rho\gamma)}{\partial t}+\frac{\partial(\rho U_j\gamma)}{\partial x_i}=P_{\gamma_1}-E_{\gamma_1}+P_{\gamma_2}-E_{\gamma_2}+\frac{\partial}{\partial x_j}\left[\left(\mu_+\frac{\mu_t}{\sigma_\gamma}\right)\frac{\partial\gamma}{\partial x_j}\right] \quad (20)$$

The transition sources are defined as

$$E_{\gamma_1}=P_{\gamma_1}\gamma \text{ and} \quad (21)$$

$$P_{\gamma_1}=F_{length}\rho S[\gamma F_{onset}]^{c_{\gamma3}} \quad (22)$$

where, S = the strain rate magnitude, F_{length} = an empirical correlation that controls the length of the transition region.

The destruction/relaminarization sources are defined as

$$P_{\gamma_2}=(2c_{\gamma1})\rho\Omega\gamma F_{turb}\text{and} \quad (23)$$

$$E_{\gamma_2}=c_{\gamma2}P_{\gamma_2}\gamma \quad (24)$$

where, Ω is the vorticity magnitude.

Model constants:

$$c_{\gamma1}=0.03,\ c_{\gamma2}=50,\ c_{\gamma3}=1.0$$

2.4 Setting Boundary Conditions

The Mach number in this study is 0.015, which is lesser than 0.3 for which the flow is considered as incompressible and therefore energy equation has been omitted in numerical simulation. The solver has been taken as pressure-based and velocity formation has been taken as absolute. The time for the flow has been set as steady. Wall boundary condition is applied for airfoil surfaces with no-slip boundary conditions. The inlet (far-field 1) is assigned as velocity inlet where the velocity specification method is taken as component and reference frame is absolute with an initial gauge pressure of 0 Pa. The specification of turbulence is taken as an intensity to viscosity ratio with a turbulence intensity of 5% and turbulence viscosity ratio of 10. The outlet (far-field 2) is assigned as a pressure outlet having a gauge pressure of 0 Pa and the backflow reference frame is set as absolute, the backflow direction specification method is set as normal to the boundary, and the backflow pressure specification is set as total pressure. Fig. 4 illustrates the flow domain of the problem. Boundary conditions and other variables related to the numerical investigation are tabulated in Table 1.

2.5 Simulation Setup

The SIMPLE pressure-velocity coupling has been used in the present study. For spatial discretization, the gradient is taken as least square cell-based and other parameters are taken as second-order upwind. Reports have been defined to calculate lift and drag coefficients. The convergence condition is taken as absolute criteria. The criterion of the residuals is taken as 10^{-6}. The solution is initialized with the standard initialization method. Then the calculation is, then, run to get quantitative and qualitative numerical results.

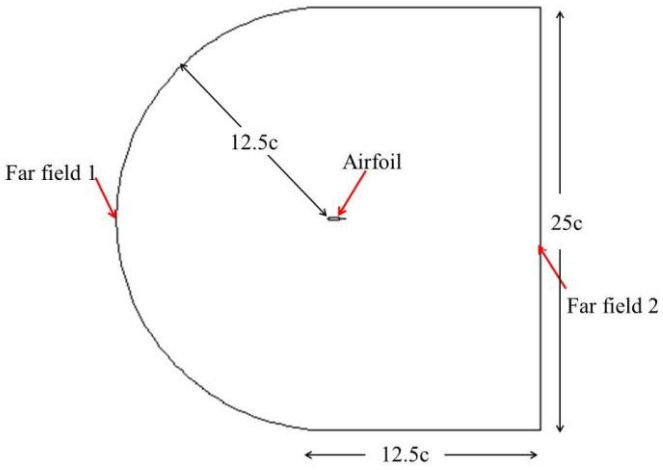

Fig. 4 Flow domain of the problem.

Table 1 Boundary conditions and some other variables.

Variable	Value
Fluid type	air
Test object material	wood
Free stream temperature	20 °C
Gauge pressure	0 Pa
Free stream velocity of air	5 m/s
Density of air	1.204 kg/m^3
Viscosity of air	1.825×10^{-5} kg·m^{-1}·s^{-1}
Chord Reynolds number	0.05×10^6
Mach number	0.015

2.6 Wind Tunnel Experiment

The wind tunnel experiment has been conducted using a subsonic open-circuit wind tunnel consisting of a converging and diverging nozzle to verify the performance of the turbulence models. The specification of the wind tunnel is presented in Table 2.

The models for both of the airfoils have been made of wood with having a chord of 150 mm and a span of 450 mm. The models have been fabricated and provided a smooth surface finish and thick coating so that the output obtained from wind tunnel testing is more accurate. Fig. 5 shows the wind tunnel with an airfoil mounted on it. In this present study, the free stream velocity is taken as 5 m/s for both of the airfoils which yield a Reynolds number of 0.05×10^6 and Mach number of 0.015 based on the centerline chord of the airfoils. The velocity of air is increased up to 5 m/s and was inspected by a monitor.

Table 2 Specifications of the wind tunnel.

Specifications	Value
Model	TecQuipment AF100
Electrical supply	3 phase, 220 VAC to 240 VAC 50 Hz/60 Hz (20 A) or 380 VAC to 440 VAC 50 Hz/60 Hz (16 A)
Space required	2 m of free space around the inlet and 4 m at the outlet
Operating temperature range	5 °C to 40 °C
Operating relative humidity range	80% at temperatures < 31°C decreasing linearly to 50% at 40°C.
Net dimensions	3700 mm × 1065 mm × height 1900 mm
Dimensions of the working section	305 mm × 305 mm, and 600 mm long
Net weight	293 kg
Range of air velocity	0 to 36 ms^{-1}
Noise level	80 dB(A)

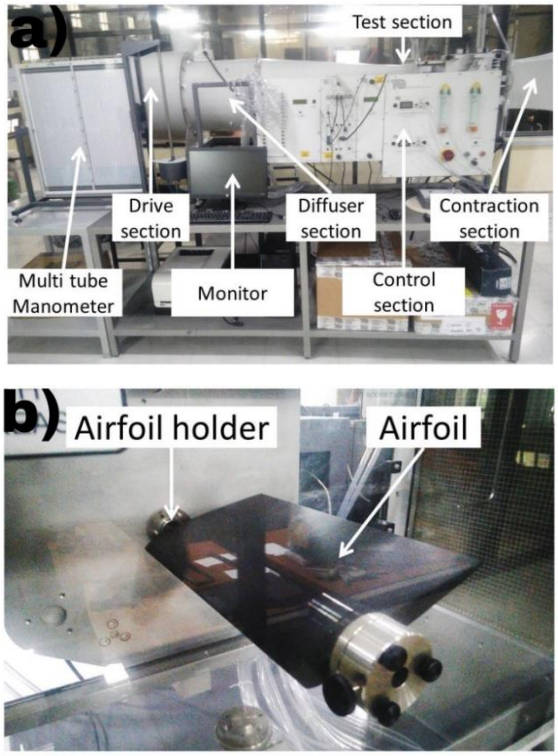

Fig. 5 Experimental setup showing (a) whole experimental setup and (b) close view of airfoil setup.

Lift and drag force are obtained using wind tunnel testing for both of the airfoils. Lift coefficient and drag coefficient are determined from these aerodynamic forces using Eqs. (25) and (26) respectively.

$$C_L = \frac{F_L}{\frac{1}{2}\rho v^2 A} \tag{25}$$

$$C_D = \frac{F_D}{\frac{1}{2}\rho v^2 A} \tag{26}$$

Where, F_L is lift force in N, F_D is drag force in N, C_L is lift coefficient, C_D is drag coefficient, ρ is the density of the air through the airfoil is moving in kg/m^3, v is the relative speed between airfoil and air in m/s and A is the projected area of the airfoil in m^3.

In order to monitor experimental results such as lift coefficient and drag coefficient at a different angle of attack for both of the airfoils, computer along with TecQuipment's Versatile Data Acquisition System (VDAS®) software is used. With the usage of VDAS® software, lift coefficient and drag coefficient are accurately determined.

3 Results and discussion

3.1 Evaluation of turbulence models for the flow over NACA 0012 airfoil

Fig. 6 illustrates a comparison between experimental data and numerical results of five different turbulence models of the lift coefficient curve for NACA 0012 airfoil. It is observed that Spalart-Allmaras model and k-ω SST model are able to reasonably predict lift coefficient up to the angle of attack of 9° and 6° respectively. Hence, it is obvious that Spalart-Allmaras model gives the most accurate prediction among other models. This finding is closely in agreement with previous studies conducted on the accuracy of turbulence models [6],[7],[9],[10]. The standard k-ε model gives slightly less value of lift coefficient at low angle of attack and slightly high value of lift coefficient at high angle of attack. However, at high angle of attack no turbulence model is capable of providing a satisfactory prediction. This phenomenon is also confirmed by prior studies [10],[11]. Transition k-k_L-ω model and $\gamma - Re_\theta$ Transition SST model are far beyond accuracy.

Fig. 7 demonstrates a comparison between experimental data and numerical results of five different turbulence models of the drag coefficient curve for NACA 0012 airfoil. It is observed that k-ω SST model, Spalart-Allmaras model, Transition k-k_L-ω model, and $\gamma - Re_\theta$ Transition SST model can predict drag coefficient reasonably at low angle of attack. The standard k-ε model gives slightly high value of drag coefficient at a low angle of attack and a slightly low value of drag coefficient at a high angle of attack. However, at a high angle of attack, no turbulence model can give a satisfactory prediction and all models except the Transition k-k_L-ω model provide a lesser value of drag coefficient than that of the experimental value. Previous studies also indicate that turbulence models aren't capable of predicting at a high angle of attack [10],[11].

Fig. 8 and Fig. 9 illustrate contours of static pressure at the angle of attack of 0°, 6°, 9°, and 18° derived from Spalart-Allmaras model and k-ω SST model respectively for NACA 0012 airfoil. It can be observed that pressure distribution is symmetrical at 0° angle of attack because of NACA 0012 being symmetric airfoil while the pressure on the upper surface is lower than that of the lower surface at 6° and 9° angle of attack. Hence, a lift is produced upward. As the angle of attack is increased from 0° up to 9°, the pressure on the lower surface is increased as a result of which the lift force and lift coefficient are increased in the upward direction. However, separation takes place at an angle of attack of 18° due to which the lift coefficient is dramatically decreased.

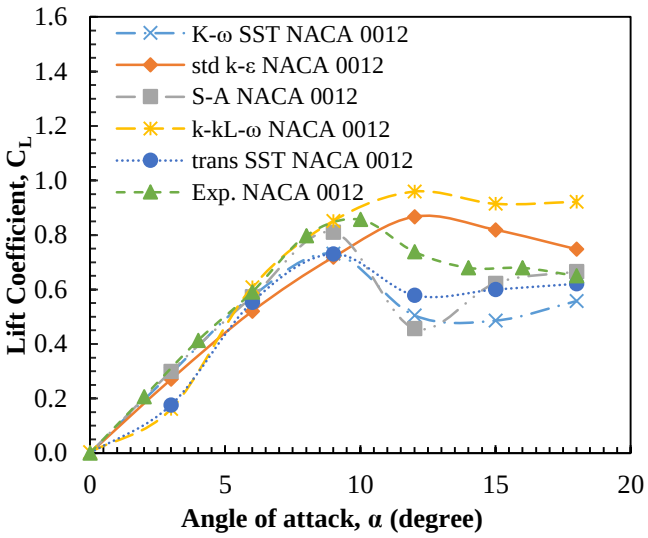

Fig. 6 Comparison between experiment data and numerical results of five different turbulence models of the lift coefficient curve for NACA 0012 airfoil.

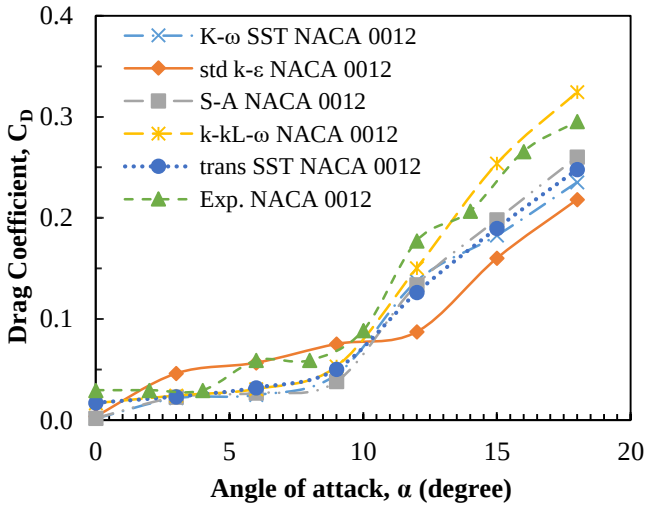

Fig. 7 Comparison between experiment data and numerical results of five different turbulence models of the drag coefficient curve for NACA 0012 airfoil.

Fig. 10 and Fig. 11 demonstrate contours of velocity magnitude at the angle of attack of 0°, 6°, 9° and 18° for Spalart-Allmaras model and k-ω SST model respectively for NACA 0012 airfoil. It can be observed that velocity magnitude is symmetrical at 0° angle of attack while in contrast to pressure distribution the velocity magnitude on the upper surface is higher than that of the lower surface for increased angle of attack which confirms Bernoulli's principle. The stagnation point at the trailing edge is moved forward to the direction of the leading edge with the increase in the angle of attack.

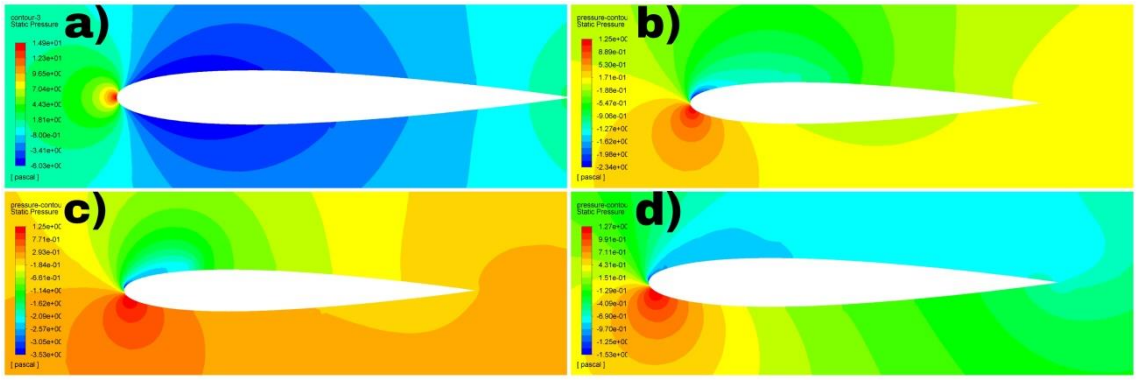

Fig. 8 Contours of static pressure at an angle of attack of (a) 0°, (b) 6°, (c) 9°, (d) 18° derived from Spalart-Allmaras model for NACA 0012 airfoil.

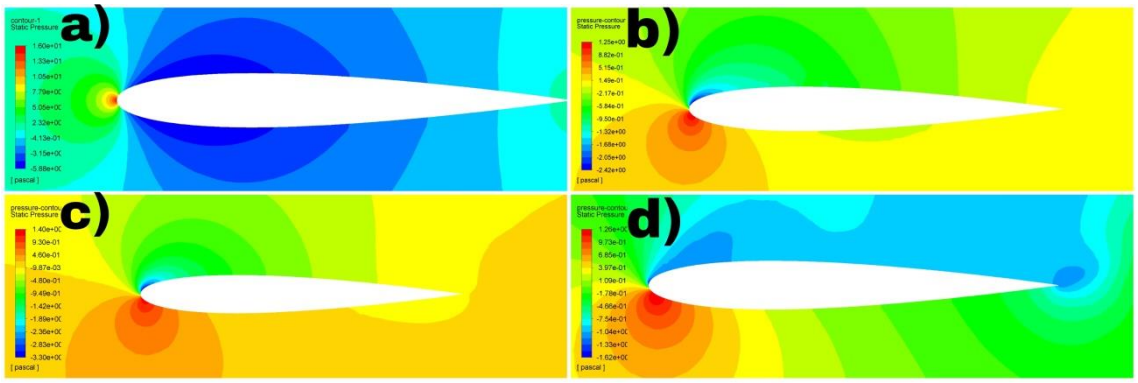

Fig. 9 Contours of static pressure at an angle of attack of (a) 0°, (b) 6°, (c) 9°, (d) 18° derived from k-ω SST model for NACA 0012 airfoil.

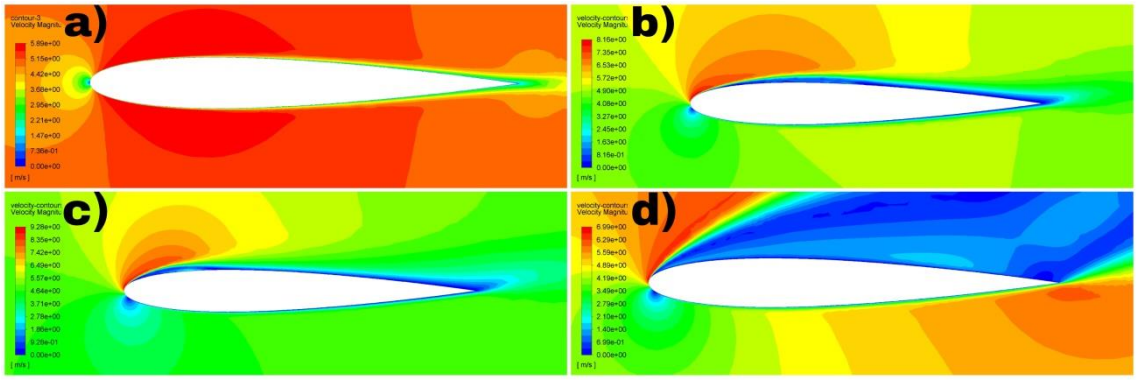

Fig. 10 Contours of velocity magnitude at an angle of attack of (a) 0°, (b) 6°, (c) 9°, (d) 18° derived from Spalart-Allmaras model for NACA 0012 airfoil.

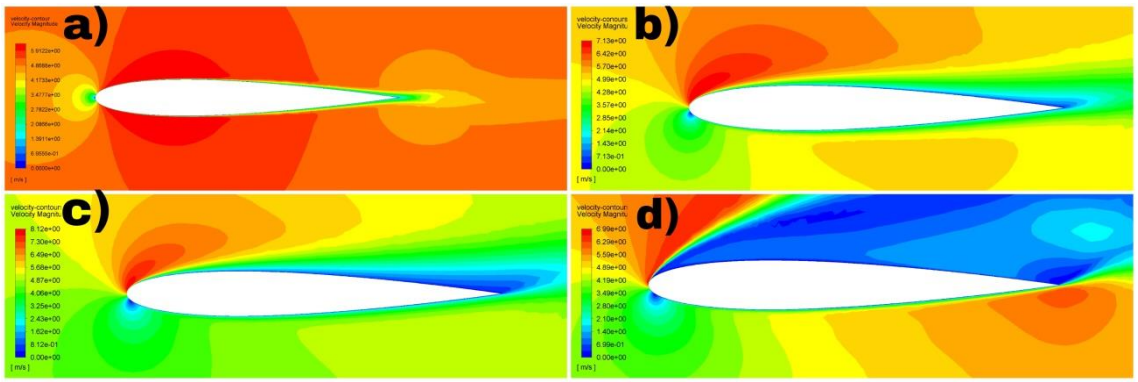

Fig. 11 Contours of velocity magnitude at an angle of attack of (a) 0°, (b) 6°, (c) 9°, (d) 18° derived from k-ω SST model for NACA 0012 airfoil.

3.2 Evaluation of turbulence models for the flow over NACA 2412 airfoil

Fig. 12 illustrates a comparison between experimental data and numerical results of five different turbulence models of the lift coefficient curve for NACA 2412 airfoil. It is observed that Spalart-Allmaras model and k-ω SST model are successfully able to predict lift coefficient up to the angle of attack of 9°. This finding is closely in agreement with earlier studies conducted on the assessment of turbulence models [6],[7],[9],[10]. Standard k-ε model gives slightly less value of lift coefficient at low angle of attack and slightly more value of lift coefficient at high angle of attack. However, no turbulence model is able to depict post-stall characteristics. Transition k-k_L-ω model and $\gamma - Re_\theta$ transition SST model are far beyond accuracy.

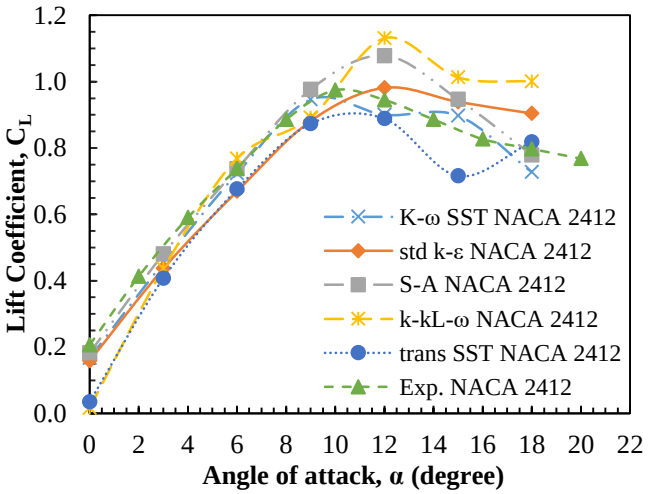

Fig. 12 Comparison between experiment data and numerical results of five different turbulence models of the lift coefficient curve for NACA 2412 airfoil.

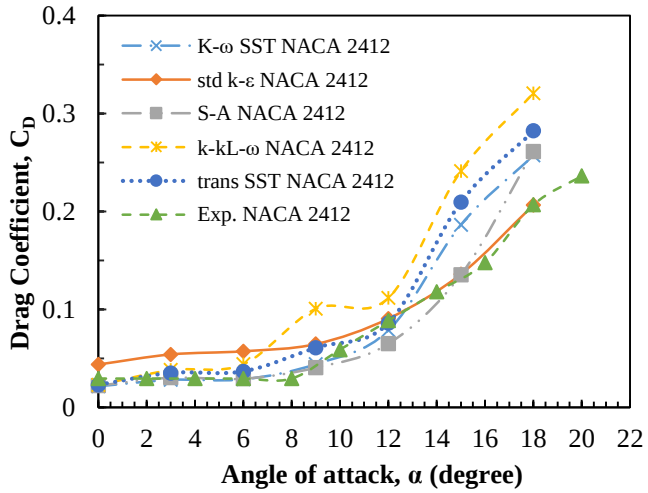

Fig. 13 Comparison between experiment data and numerical results of five different turbulence models of the drag coefficient curve for NACA 2412 airfoil.

Fig. 13 illustrates a comparison between experimental data and numerical results of five different turbulence models of the drag coefficient curve for NACA 2412 airfoil. It is observed that k-ω SST model, Spalart-Allmaras model, Transition k-k_L-ω model and $\gamma - Re_\theta$ Transition SST model are capable of predicting drag coefficient effectively at a low angle of attack. The standard k-ε model gives slightly high value of drag coefficient at a low angle of attack and exhibits a good prediction of drag coefficient at a high angle of attack. However, at a high angle of attack, no turbulence model can give a satisfactory prediction except the Standard k-ε model and they give higher value of drag coefficient than that of the experimental value. Douvi et al. [10] also observed that higher drag coefficients than that of the experimental result were deduced by different turbulence models.

Contours of static pressure at the angle of attack of 0°, 6°, 9° and 18° derived from Spalart-Allmaras model and k-ω SST model are demonstrated at Fig. 14 and Fig. 15 respectively for NACA 2412 airfoil. It can be observed that the pressure on the upper surface is lower than that of the lower surface because of which a lift is produced upward. As the angle of attack is increased from 0° to 9°, the pressure on the lower surface is increased as a result of which the lift force and lift coefficient are increased in the upward direction. However, separation takes place at an angle of attack of 18° due to which the lift coefficient is dramatically decreased.

Contours of velocity magnitude at the angle of attack of 0°, 6°, 9° and 18° for Spalart-Allmaras model and k-ω SST model are illustrated at Fig. 16 and Fig. 17 respectively for NACA 2412 airfoil. It can be observed that, unlike pressure distribution, the velocity magnitude on the upper surface is higher than that of the lower surface, which confirms Bernoulli's principle. The stagnation point at the trailing edge is moved forward to the direction of the leading edge with the increase in the angle of attack.

3.3 Comparison of NACA 0012 and NACA 2412 using experimental results

Fig. 18 illustrates a variation of lift coefficient with respect to the angle of attack for both NACA 0012 and NACA 2412 airfoils. It is observed that at a low angle of attack the lift coefficient increases almost linearly with the angle of attack and reaches its highest value at stall angle of attack (10°) because airflow is attached to the surfaces of airfoils at these angles of attack. After stall angle of attack, there is a dramatic decrease in lift coefficient because of the separation of the boundary layer. It can also be observed that the lift coefficient of NACA 2412 airfoil is greater than that of the NACA 0012 airfoil for all angles of attack. It was also depicted by Oukassou et al. [9] that NACA 2412 airfoil provided greater lift coefficients for a wide range of angles of attack at a Reynolds number of 10^6. Hence, NACA 2412 airfoil provides better aerodynamic performance. The lift coefficient is zero lift for 0° angle of attack for NACA 0012 airfoil while there is an appreciable lift coefficient at 0° angle of attack for NACA 2412 airfoil.

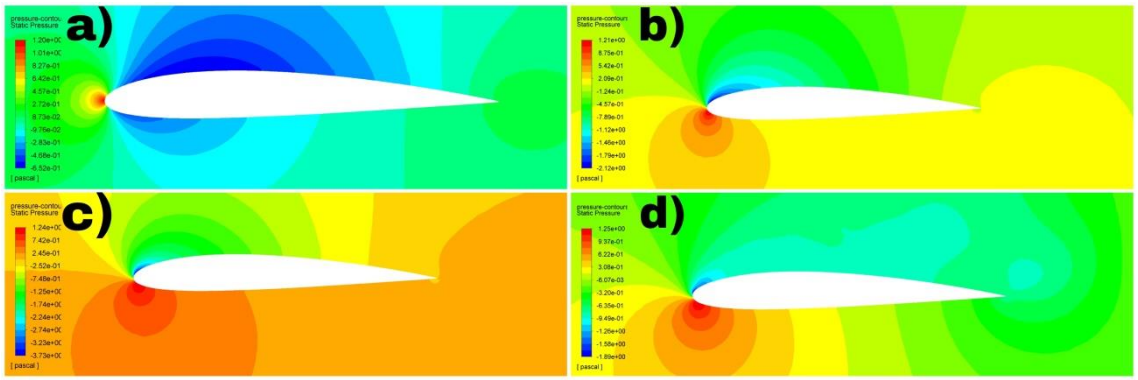

Fig. 14 Contours of static pressure at an angle of attack of (a) 0°, (b) 6°, (c) 9°, (d) 18° derived from Spalart-Allmaras model for NACA 2412 airfoil.

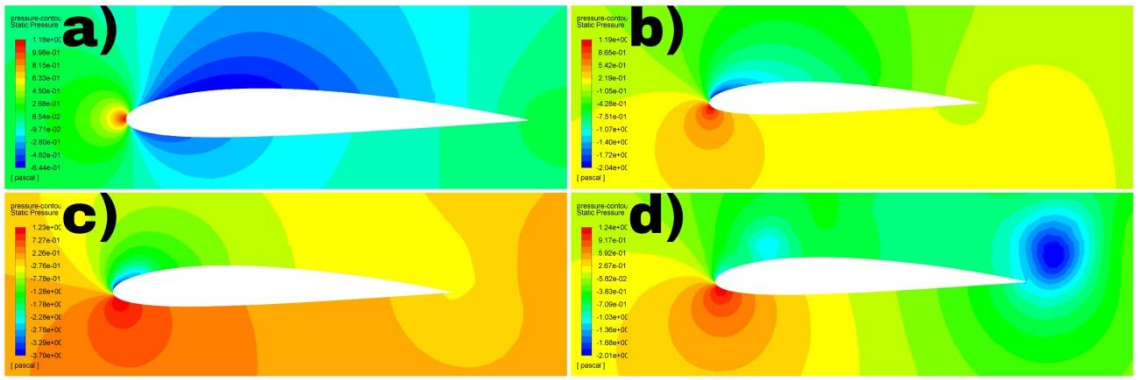

Fig. 15 Contours of static pressure at an angle of attack of (a) 0°, (b) 6°, (c) 9°, (d) 18° derived from k-ω SST model for NACA 2412 airfoil

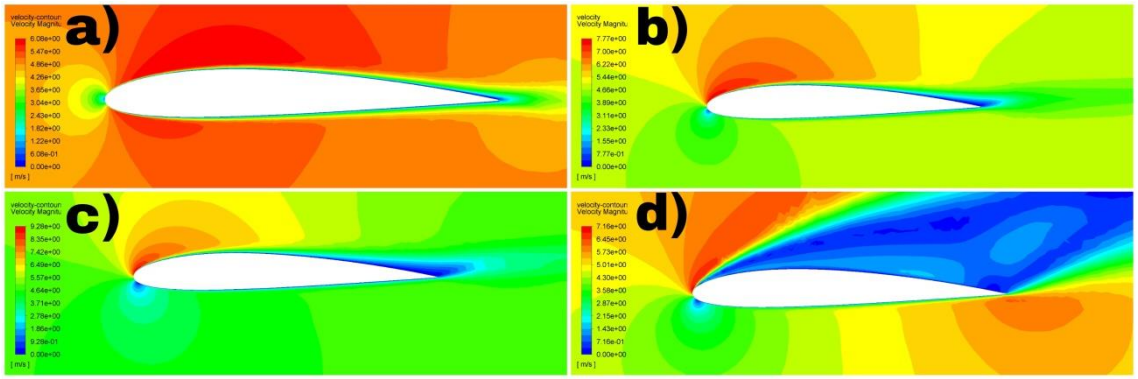

Fig. 16 Contours of velocity magnitude at an angle of attack of (a) 0°, (b) 6°, (c) 9°, (d) 18° derived from Spalart-Allmaras model for NACA 2412 airfoil.

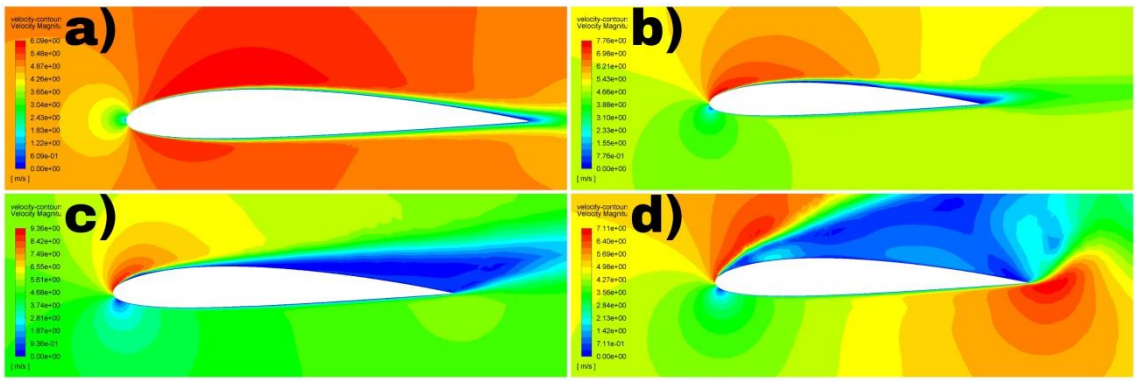

Fig. 17 Contours of velocity magnitude at an angle of attack of (a) 0°, (b) 6°, (c) 9°, (d) 18° derived from k-ω SST model for NACA 2412 airfoil.

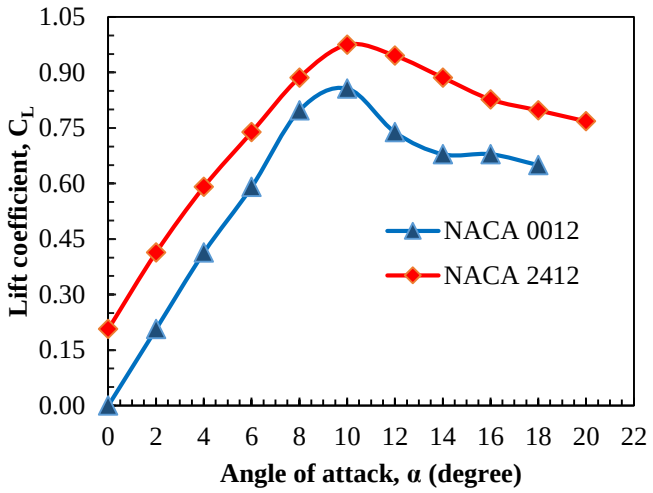

Fig. 18 Comparison of lift coefficient between NACA 0012 and NACA 2412 airfoils using experimental data.

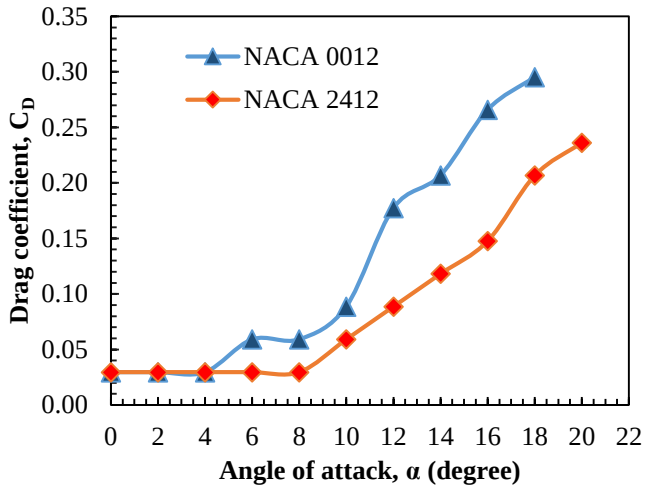

Fig. 19 Comparison of drag coefficient between NACA 0012 and NACA 2412 airfoils using experimental data.

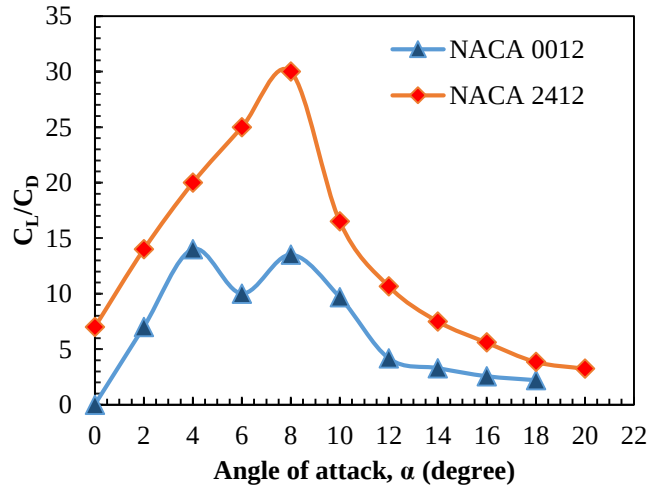

Fig. 20 Comparison of lift coefficient to drag coefficient ratio between NACA 0012 and NACA 2412 airfoils using experimental data.

Fig. 19 demonstrates the variation of drag coefficient with respect to the angle of attack for both NACA 0012 and NACA 2412 airfoils. It can be observed that at a low angle of attack the drag coefficient varies a little bit with respect to the angle of attack since only skin friction drag is affecting the airfoils while the pressure drag is negligible. After stall angle of attack, there is a rapid increase in drag coefficient which is due to separation of flow, which enhances pressure drag, and thus total drag is increased. It is also observed that the drag coefficient of NACA 0012 is higher than that of NACA 2412 airfoil at almost all angles of attack.

Fig. 20 illustrates the variation of lift coefficient to drag coefficient ratio with respect to the angle of attack for both NACA 0012 and NACA 2412 airfoils. It can be observed that the lift coefficient to drag coefficient ratio of NACA 2412 is higher than that of NACA 0012 airfoil for all angles of attack. The ratio increases from zero angle of attack to the angle of attack of 8° for NACA 2412 airfoil and 4° for NACA 0012 airfoil and after that lift coefficient to drag coefficient ratio gradually falls. The lift coefficient to drag coefficient ratio of NACA 2412 airfoil is greater than that of the NACA 0012 airfoil which indicates that NACA 2412 airfoil is more fuel economic.

4 Conclusions

This paper has presented the evaluation of five different turbulence models at low Reynolds number as well as the aerodynamic comparison between NACA 0012 airfoil and NACA 2412 airfoil for various angles of attack. The findings of this study can be concluded as follow:

Spalart-Allmaras model and k-ω SST model are capable of providing the most accurate prediction for lift coefficient at low angle of attack for both airfoils. k-ω SST model, Spalart-Allmaras model, Transition k-k_L-ω model, and $\gamma - Re_\theta$ transition SST model can predict drag coefficient reasonably at a low angle of attack. At a high angle of attack, however, no turbulence model is able to provide a satisfactory prediction for lift coefficient and drag coefficient indicating that these models are unable to predict post-stall characteristics. NACA 2412 airfoil provides better aerodynamic performance. Moreover, NACA 2412 is more fuel economic. NACA 0012 airfoil provides zero lift at an angle of attack of 0° while NACA 2412 airfoil provides appreciable lift at an angle of attack of 0°. The stall angle of attack for both of the airfoils is found to be the same *ie.* 10°.

Acknowledgments

The authors are grateful to Fluid Machinery Lab, Chittagong University of Engineering & Technology for providing the laboratory facility.

References

[1] Patel, K.S., Patel, S.B., Patel, U.B. and Ahuja, A.P., 2014. CFD Analysis of an Aerofoil. *International Journal of Engineering Research*, *3*(3), pp.154-158.

[2] Pranto, M.R.I. and Inam, M.I., 2020. Numerical Analysis of the Aerodynamic Characteristics of NACA4312 Airfoil. *Journal of Engineering Advancements*, *1*(02), pp.29-36.

[3] Mubassira, S., Muna, F.I. and Inam, M.I., 2021. Numerical Investigation of Aerodynamic Characteristics of NACA 4312 Airfoil with Gurney Flap. *Journal of Engineering Advancements*, *2*(02), pp.63-70.

[4] Milne-Thomson, L.M., 1973. *Theoretical aerodynamics*. Courier Corporation.

[5] McLay, A., 1995. Computational Fluid Dynamics: the Basics with Applications, JD Anderson, McGraw-Hill Book Company.

[6] Sahoo, S. and Maity, S., 2020. CFD Analysis of Responses of Two-Equation Turbulence Models for Flow over NACA 0012, NACA 4412 and S809 Aerofoils. In *Advances in Mechanical Engineering* (pp. 31-40). Springer, Singapore.

[7] El Maani, R., Radi, B. and El Hami, A., CFD Analysis of the Transonic Flow over a NACA 0012 Airfoil. Published by ISTE Ltd. London, UK.

[8] Badran, O., Aldudak, R.Q.F. and und Aerodynamik, F.S., Two-Equation Turbulence Models for Turbulent Flow over a NACA 4412 Airfoil at Angle of Attack 15 Degree. *Mechanical Engineering Department, Faculty of Engineering technology, Al-Balqa Applied University, Jordan*.

[9] Oukassou, K., El Mouhsine, S., El Hajjaji, A. and Kharbouch, B., 2019. Comparison of the power, lift and drag coefficients of wind turbine blade from aerodynamics characteristics of Naca0012 and Naca2412. *Procedia Manufacturing*, *32*, pp.983-990.

[10] Eleni, D.C., Athanasios, T.I. and Dionissios, M.P., 2012. Evaluation of the turbulence models for the simulation of the flow over a National Advisory Committee for Aeronautics (NACA) 0012 airfoil. *Journal of Mechanical Engineering Research*, *4*(3), pp.100-111.

[11] Linjing, M.A., Jiang, C., Gang, D.U. and Renjing, C., 2010. Numerical simulation of aerodynamic performance for wind turbine airfoils. *Acta Energiae Solaris Sinica*., *2*, pp.203–209.

[12] Bacha, W. and Ghaly, W., 2006. Drag prediction in transitional flow over two-dimensional airfoils. In *44th AIAA AeroSpace Sciences Meeting and Exhibit* (p. 248).

[13] Sogukpinar, H., 2018, February. The effects of NACA 0012 airfoil modification on aerodynamic performance improvement and obtaining high lift coefficient and post-stall airfoil. In *AIP conference proceedings* (Vol. 1935, No. 1, p. 020001). AIP Publishing LLC.

[14] Saxena, E.S. and Kumar, M.R., 2015. Design of NACA 2412 and its Analysis at Different Angle of Attacks, Reynolds Numbers, and a wind tunnel test. *International Journal of Engineering Research and General Science*, *3*(2), pp.193-200.

[15] Mayer, Y., Zang, B. and Azarpeyvand, M., 2019. Aeroacoustic characteristics of a NACA 0012 airfoil for attached and stalled flow conditions. In *25th AIAA/CEAS Aeroacoustics Conference* (p. 2530).

[16] Harish, H.V., Arundeep, M., Santhosh, N., 2019. Prediction Of Stalling Angle By Analysis Of Flow Over Symmetric Aerofoil. *Journal of Engineering Science and Technology 2*(2), pp.17-28.

[17] Patil, B.S. and Thakare, H.R., 2015. Computational fluid dynamics analysis of wind turbine blade at various angles of attack and different Reynolds number. *Procedia Engineering*, *127*, pp.1363-1369.

[18] Hasegawa, M. and Sakaue, H., 2017. Drag reduction using hairy chemical coating on NACA 0012 airfoil in turbulent airflow. In *55th AIAA Aerospace Sciences Meeting* (p. 0283).

[19] Venkatesan, S.P., Kumar, V.P., Kumar, M.S. and Kumar, S., 2018. Computational analysis of aerodynamic characteristics of dimple airfoil NACA 2412 at various angles of attack. *Idea*, *46*, p.10.

[20] Meghani, P., 2018. A 2D Aerodynamic Study on Morphing in The NACA 2412 Aerofoil. In *13th Research and Education in Aircraft Design Conference, Brno, Czech Republic*.

[21] Havaldar, S.N., Pawar, S., Lele, A., Pradhan, R. and Rishi, A., Experimental Investigation of Lift forNACA 2412 Airfoil without Internal Passage with NACA 2412 Airfoil with Internal Passage in a Subsonic Wind Tunnel. *Journal of Aerospace Engineering & Technology*, *5*(2), pp.27-33.

[22] ANSYS Fluent 2019 R2. 2019.

[23] Wilcox, D.C., 1988. Reassessment of the scale-determining equation for advanced turbulence models. *AIAA journal*, *26*(11), pp.1299-1310.

[24] Menter, F.R., 1994. Two-equation eddy-viscosity turbulence models for engineering applications. *AIAA journal*, *32*(8), pp.1598-1605.

[25] Launder, B.E., Spalding, D.B., 1974. The numerical computation of turbulent flows. Computer Methods in Applied Mechanics and Engineering. *3*(2), pp.269–289.

[26] Shih, T.H., Liou, W.W., Shabbir, A., Yang, Z. and Zhu, J., 1995. A new k-ϵ eddy viscosity model for high reynolds number turbulent flows. *Computers & fluids*, *24*(3), pp.227-238.

[27] Spalart, P. and Allmaras, S., 1992, January. A one-equation turbulence model for aerodynamic flows. In *30th Aerospace Sciences Meeting and Exhibit* (p. 439).

[28] Walters, D.K. and Cokljat, D., 2008. A three-equation eddy-viscosity model for Reynolds-averaged Navier–Stokes simulations of transitional flow. *Journal of Fluids Engineering*, *130*(12).

[29] Walters, D.K. and Leylek, J.H., 2004. A new model for boundary layer transition using a single-point RANS approach. *J. Turbomach.*, *126*(1), pp.193-202.

[30] Langtry, R. and Menter, F., 2005, January. Transition modeling for general CFD applications in aeronautics. In *43rd AIAA Aerospace Sciences Meeting and Exhibit* (p. 522).

[31] Menter, F.R., Langtry, R. and Völker, S., 2006. Transition modelling for general purpose CFD codes. *Flow, Turbulence and Combustion*, *77*(1), pp.277-303.

[32] Langtry, R.B. and Menter, F.R., 2009. Correlation-based transition modeling for unstructured parallelized computational fluid dynamics codes. *AIAA Journal*, *47*(12), pp.2894-2906.

[33] Contigiani, C.C., Colli, A.N., Pérez, O.G. and Bisang, J.M., 2020. The effect of a conical inner electrode on the mass-transfer behavior in a cylindrical electrochemical reactor under single-phase and two-phase (Gas-Liquid) swirling flow. *Journal of The Electrochemical Society*, *167*(8), p.083501.